

# A Transient Thermal Model for Friction Stir Weld. Part II: Effects of Weld Conditions

X.X. ZHANG, B.L. XIAO, and Z.Y. MA

In Part II of this series of articles, the transient thermal model, which was introduced in Part I, is used to explore the effects of welding conditions on the heat generation and temperature. FSW of the 6061-T651 aluminum alloy is modeled to demonstrate the model. The following two steps are adopted to study the influence of welding conditions on the heat generation and temperature. First, the thermal model is used to compute the heat generation and temperature for different welding conditions, the calculated results are compared with the reported experimental temperature, and a good agreement is observed. Second, the analytical method is used to explore the approximate functions describing the effect of welding conditions on the heat generation and temperature. Based on the computed results, we discuss the relationship between the welding conditions, heat generation, temperature, and friction coefficient, and propose a relationship map between them for the first time at the end.

DOI: 10.1007/s11661-011-0730-z

© The Minerals, Metals & Materials Society and ASM International 2011

## I. INTRODUCTION

THERE is a wide range of fascinating questions<sup>[1]</sup> related to understanding the relationship between welding conditions, thermal values (heat generation and temperature), microstructural evolution, and mechanical properties in friction stir welds (FSWs). In the past decade, many researchers<sup>[2–11]</sup> have studied this relationship. It was reported that rotation rate, advancing speed, and tool geometry exerted significant effects on the thermal values, microstructural evolution, and mechanical properties of the FSW joints. However, in the early stages, research results did not reach an agreement in the relationship between the welding conditions and the mechanical properties of the welds.<sup>[7–11]</sup> Lee *et al.*<sup>[7]</sup> and Lim *et al.*<sup>[8]</sup> reported that decreasing the welding speed and increasing the rotation rate decreased the strength and elongation of FSW 6061Al-T651 joints. However, Ren *et al.*'s study<sup>[9]</sup> indicated that the strength of the FSW 6061Al-T651 joints did not change significantly with the variation of the rotation rate. Scialpi *et al.*<sup>[10]</sup> reported that a shoulder with a fillet and a cavity produced the best FSW 6082Al joint, whereas Fujii *et al.*<sup>[11]</sup> pointed out that the tool geometry did not exert a remarkable effect on the mechanical properties of 6061Al-T651 joints.

Recently, Liu and Ma<sup>[12]</sup> studied systematically the relationship between the FSW conditions, thermal cycles, microstructure, and hardness of the low hardness zone (LHZ) of FSW 6061-T651 aluminum alloys, and

proposed a heat source zone–isothermal dissolution layer (HSZ-ITDL) model. To quest for better understanding of the FSW process, it is important to obtain the accurate and global information of the evolution history of temperature, microstructure, and mechanical properties. However, *in-situ* experimental measurements of the FSW process are limited. It is impossible even to measure the temperature in the stir zone (SZ) because of the intense plastic deformation. Fortunately, numerical modeling, which combines thermal, microstructural, and mechanical modeling, provides a suitable way to study the relationship between the welding conditions, thermal values, microstructural evolution, and mechanical properties of the welds. To do this, thermal modeling is the first and crucial step. In the past decade, many models,<sup>[13–28]</sup> including the finite element method, computational fluid dynamics, and analytical models, have been used to explore the heat generation and temperature distribution in FSW. However, the mechanism of the effects of various welding conditions on the thermal values is not so clear.

Part I<sup>[29]</sup> has built a transient thermal model that considers the entire FSW process. It has been proved to be self-consistent, and its calculated results correspond well with the experimental results reported by Liu and Ma<sup>[12]</sup> and Sato *et al.*<sup>[5]</sup> In Part II, the model is used to study the relationship between welding conditions, heat generation, temperature, and friction coefficient. FSW of the 6061-T651 aluminum alloy is studied in the present article to demonstrate the model. The symbols and units used in this article are defined in Nomenclature.

X.X. ZHANG, Postgraduate, B.L. XIAO and Z.Y. MA, Professors, are with the Shenyang National Laboratory for Materials Science, Institute of Metal Research, Chinese Academy of Sciences, Shenyang 110016, People's Republic of China. Contact e-mail: zyma@imr.ac.cn

Manuscript submitted October 18, 2010.

Article published online May 14, 2011

## II. MODELING

The basic mathematical models of the heat generation and temperature were described in Part I.<sup>[29]</sup>

### A. Modeling of Torque and Weld Heat Input

The analytical estimation of the torque can be derived from the total heat generation based on the assumption that all the mechanical energy is transformed into thermal energy. Furthermore, the mechanical energy resulting from the advancing movement is neglected, because its quantity is small enough to be negligible compared to the rotational power.<sup>[26]</sup> Then the torque can be calculated by

$$M = \frac{Q_{\text{total}}}{2\pi\omega/60} \quad [1]$$

The welding heat input can be computed by dividing the total heat generation by the advancing speed:<sup>[20]</sup>

$$E = \frac{Q_{\text{total}}}{v/60} \quad [2]$$

### B. Dissolution Time

Sato *et al.*<sup>[4]</sup> pointed out that for 6xxx aluminum alloy, the high-temperature excursion above 523 K (250 °C) led to the dissolution of needle-shaped strengthening precipitates. Liu and Ma<sup>[12]</sup> revealed that the peak temperature in the LHZ of FSW 6061Al-T651 was ~643 K (370 °C). Based on these observations, Liu and Ma<sup>[12]</sup> defined a dissolution time, which denotes the duration above 523 K (250 °C) in the LHZ of FSW 6xxx aluminum alloys.

### C. Data Setting

FSW of the 6061-T651 aluminum alloy plates 400 mm in length, 75 mm in width, and 6 mm in thickness are simulated in this study. The set of samples studied in this article are summarized in Table I. A digital notation<sup>[12]</sup> for the FSW samples is used, where sample 24-8-1200-200 indicates that the shoulder diameter  $D_s$  is 24 mm, the pin diameter  $D_p$  is 8 mm, the rotation rate  $\omega$  is 1200 rpm, and the advancing speed  $v$  is 200 mm/min. Other parameters can be found in Part I.<sup>[29]</sup>

## III. COMPUTED RESULTS

A complete FSW process includes plunge, first dwell, weld, second dwell, and cool periods. When we study the influence of the welding conditions on the thermal values, microstructural evolution, and mechanical properties of the welds, the steady-state welding period is the vital part. Thus, all the values involved in the following parts are the steady-state values in the steady-state welding period of the FSW process.

### A. Heat Generation, Torque, and Weld Heat Input

The total heat generation, pin heat generation, and pin heat generation fraction, which are defined in Reference 29, for various welds are graphed in Figure 1. It can be seen that the total heat generation rises with increasing the rotation rate, advancing speed, shoulder diameter, and pin diameter. The pin heat generation increases with increasing the rotation rate, advancing speed, and pin diameter, but decreases with increasing the shoulder diameter. The pin heat generation fraction increases slowly from 13.8 to 14.0 pct with increasing the rotation rate from 900 to 1400 rpm. The change is so small that it can be treated as constant. Furthermore, the pin heat generation fraction nearly remains a constant value of 14.0 pct with increasing the advancing speed, decreases obviously with increasing the shoulder diameter, and increases rapidly with increasing the pin diameter. Note that the pin heat generation fraction varies between 13 and 37 pct for all the welds studied in the present article. This is in the range of 10 to 40 pct, as reported in previous studies. Schmidt *et al.* reported that the pin heat generation fraction was 14 pct in an earlier work<sup>[26]</sup> and 17 pct in a recent work.<sup>[13]</sup> Similarly, Colegrove *et al.*<sup>[30]</sup> and Shi *et al.*<sup>[31]</sup> revealed that the pin heat generation fraction was 20 and 25 pct, respectively.

The computed torque is depicted in Figure 2. Within the range of the welding conditions studied in the present article, the computed torque varies nearly linearly with changing the welding conditions. The torque decreases gently with increasing the rotation rate, while with increasing the advancing speed, shoulder diameter, and pin diameter, the torque increases slowly. Figure 2 also shows that the welding heat input increases slowly with increasing the rotation rate, shoulder diameter, and pin diameter, but decreases fast with increasing the advancing speed.

### B. Temperature Results

Figure 3 shows the peak temperature (the maximum temperature experienced by each point in the steady welding period) contours in the cross sections of the FSW 6061Al-T651 joints. No major differences concerning the characteristics of the temperature were observed between the advancing and the retreating sides. The distance between each peak temperature contour and the butting surface increases with increasing the rotation rate, increasing the shoulder diameter, and decreasing the advancing speed. The variation in the pin diameter from 6 to 10 mm impacts slightly on the peak temperature contours in the cross sections.

Table I. Samples Studied in This Article

Samples	$D_s$ (mm)	$D_p$ (mm)	$\omega$ (rpm)	$v$ (mm/min)
24-8-1400-600	24	8	1400	600
24-8-1400-400	24	8	1400	400
24-8-1400-200	24	8	1400	200
24-8-1200-200	24	8	1200	200
24-8-900-200	24	8	900	200
20-10-1400-400	20	10	1400	400
20-8-1400-400	20	8	1400	400
20-6-1400-400	20	6	1400	400
16-8-1400-400	16	8	1400	400

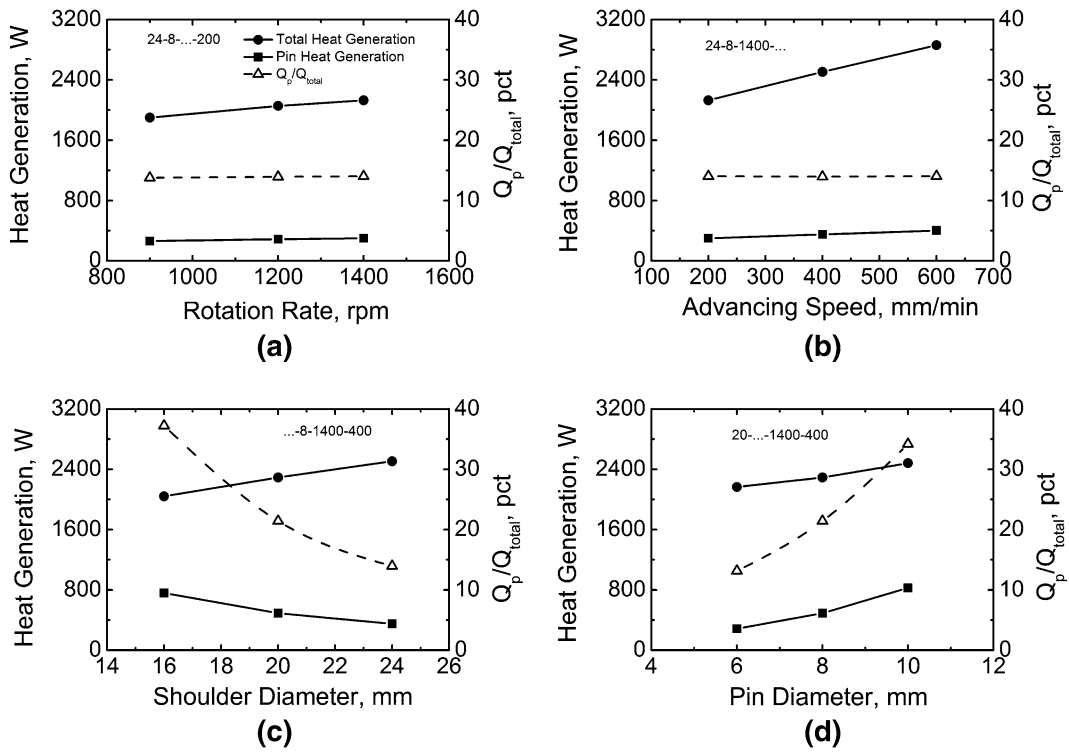


Fig. 1—Effect of welding conditions on the total heat generation, pin heat generation, and pin heat generation fraction.

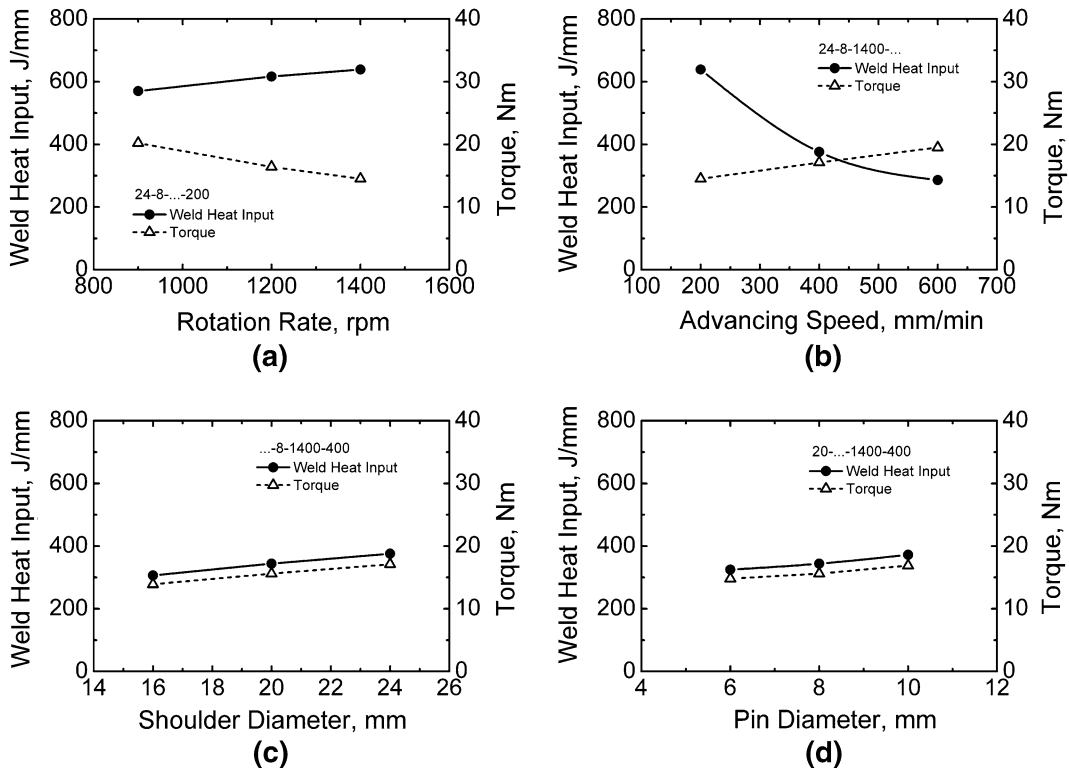


Fig. 2—Effect of welding conditions on the welding heat input and torque.

Figure 4 shows that the peak temperature for all the thermal cycles in the LHZ, whose recording position comes from Reference 12, is ~643 K (370 °C). The

dissolution time of needle-shape precipitates in the LHZ increases with increasing the rotation rate, increasing the shoulder diameter, and decreasing the advancing speed.

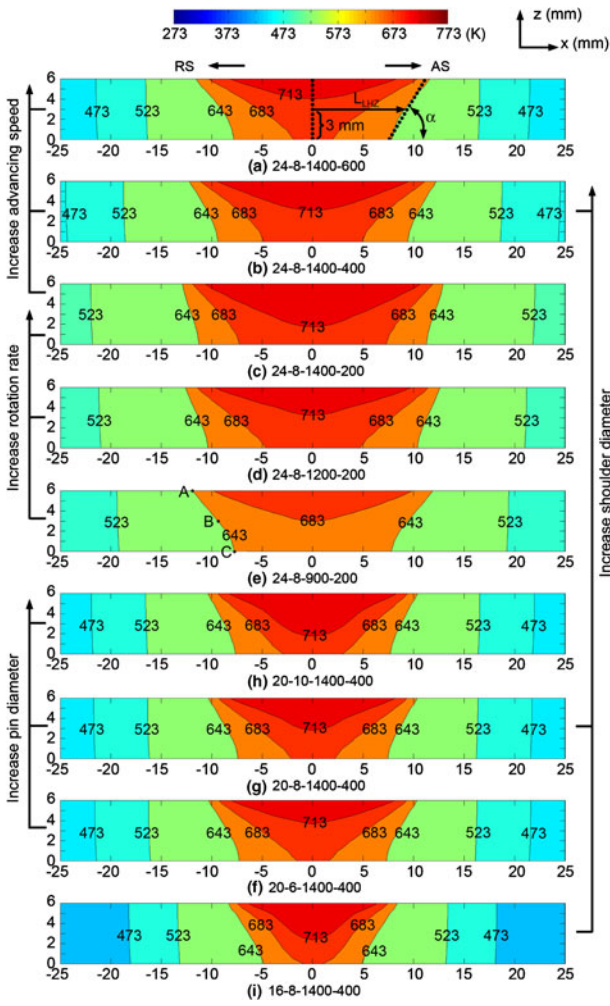


Fig. 3—Effect of welding conditions on peak temperature contours in cross sections.  $L_{LHZ}$  is the characteristic length between the 643 K (370 °C) temperature contour and butting surface.  $\alpha$  is the angle between the 643 K (370 °C) temperature contour and bottom surface.

However, the influence of the pin diameter on the dissolution time of the needle-shape precipitates in the LHZ is very small. It can be seen that the computed results agree well with the reported experimental data.<sup>[12]</sup>

Figure 5 gives the maximum temperature, the temperature in the shoulder center (SC), and temperature in the pin center (PC), respectively. The maximum temperature (a) increases slowly with increasing the rotation rate from 900 to 1400 rpm, (b) decreases slowly with increasing the advancing speed from 200 to 600 mm/min, (c) keeps almost constant with increasing the shoulder diameter, and (d) increases slowly with increasing the pin diameter. The SC and PC temperatures show the same variation trend.

#### IV. DISCUSSION

The numerical method can solve complicated functions that are difficult to be solved by the analytical method. However, a numerical solution is discrete, which means that if we want to study the effect of one

variable on the target variable, we need to calculate several times to obtain the results and then analyze them. On the other hand, the analytical method can solve relatively easy functions. Its solution is given by a formula that shows clearly the relationship between independent and dependent variables. In the present article, we try to combine the advantages of both methods. First, we study the effect of the welding parameters on the thermal values systematically and obtain their discrete results by using the thermal model. Then we derive the approximate analytical equation of the relationship between the welding parameters and the thermal values.

##### A. Relationship between Welding Parameters and Heat Generation

As the heat generation is directly connected with the temperature and energy input, it is necessary to find the effect of the welding conditions on the heat generation. Here, we consider the total heat generation and pin heat generation fraction.

When the heat generation is computed by the analytical method, the mechanical energy resulting from the advancing movement is neglected for simplifying the computation because its quantity is small enough to be negligible compared to the rotational power.<sup>[26]</sup> So the shoulder heat generation and the pin heat generation described in Part I<sup>[29]</sup> may be rewritten as

$$Q_s = \int_0^{2\pi} \int_{R_p}^{R_s} \mu(T) p \frac{2\pi\omega}{60} r^2 dr d\theta \quad [3]$$

$$Q_p = \int_0^{2\pi} \int_0^{R_p} \mu(T) p \frac{2\pi\omega}{60} r^2 dr d\theta + \int_0^{2\pi} \int_0^{\beta h_p} \mu(T) p \frac{2\pi\omega}{60} R_p^2 dz d\theta \quad [4]$$

By applying the *first mean value theorem for integration*, combined with the formula of heat generation rate, Eqs. [3] and [4] may be rewritten as

$$Q_s = \frac{\pi^2 \omega p}{45} \mu(\bar{T}_s) (R_s^3 - R_p^3) \quad [5]$$

$$Q_p = \frac{\pi^2 \omega p}{45} \mu(\bar{T}_p) (R_p^3 + 3\beta R_p^2 h_p) \quad [6]$$

Combining Eqs. [5] and [6], we obtain the total heat generation:

$$Q_{\text{total}} = \frac{\pi^2 \omega p}{45} \mu(\bar{T}_s) (R_s^3 - R_p^3) + \frac{\pi^2 \omega p}{45} \mu(\bar{T}_p) (R_p^3 + 3\beta R_p^2 h_p) \quad [7]$$

By defining a *tool friction factor*,

$$\phi = \frac{\mu(\bar{T}_s)}{\mu(\bar{T}_p)} \quad [8]$$

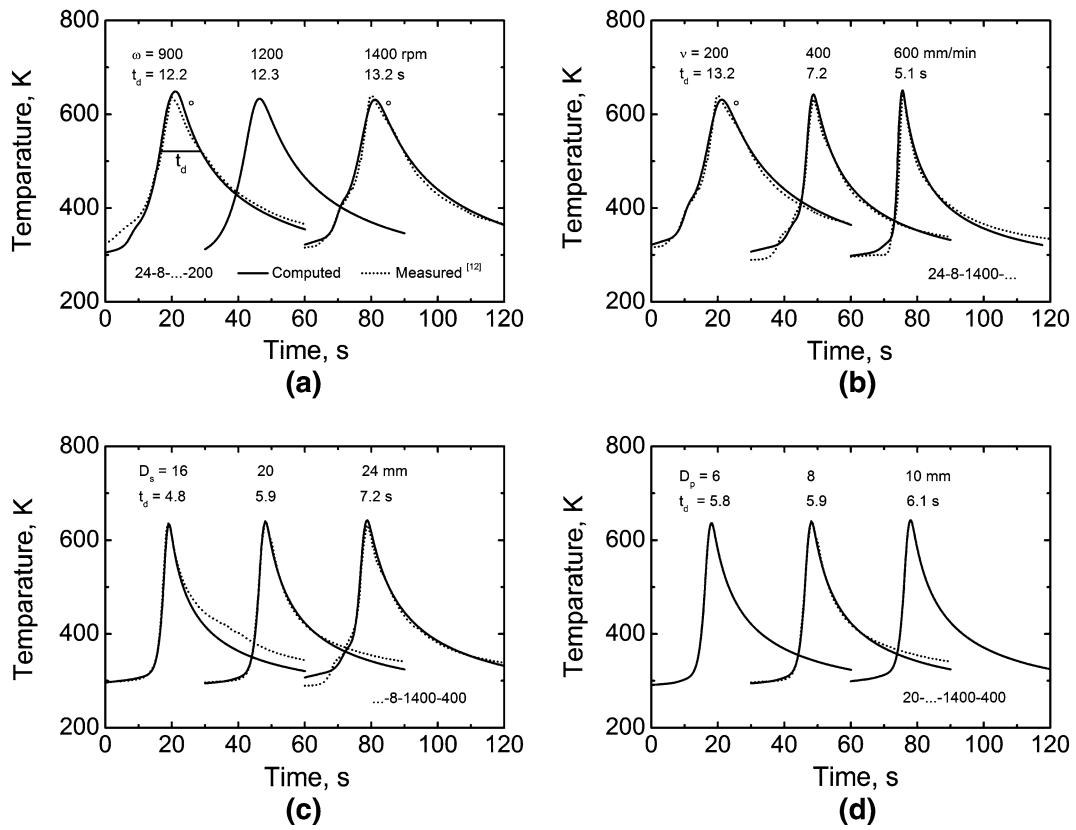


Fig. 4—Effect of welding parameters on thermal cycles in LHZ. Computed data of samples 24-8-900-200 and 24-8-1400-200 (marked by small circles) are derived from Part I,<sup>[29]</sup> while experimental results are reported by Liu and Ma.<sup>[12]</sup>

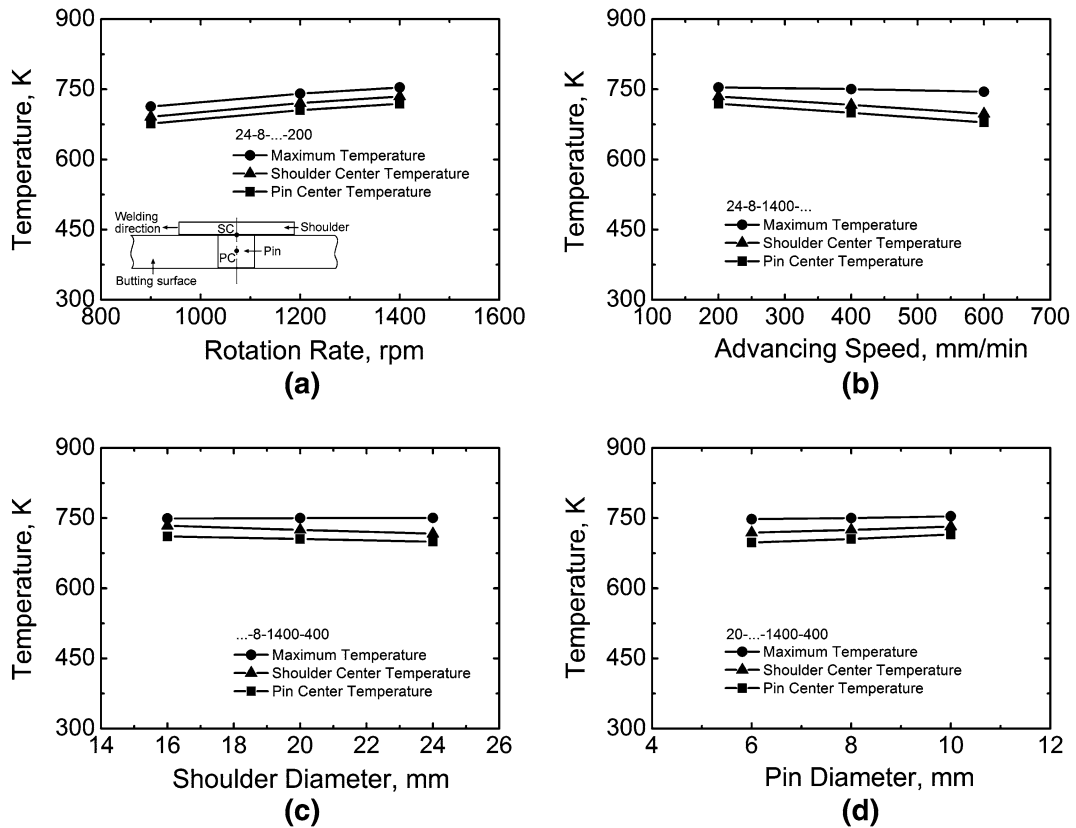


Fig. 5—Effect of welding parameters on the calculated maximum temperature, SC temperature, and PC temperature.

the total heat generation is written as

$$Q_{\text{total}} = \frac{\pi^2 \omega p}{45} \mu(\bar{T}_p) \left[ \phi \left( R_s^3 - R_p^3 \right) + \left( R_p^3 + 3\beta R_p^2 h_p \right) \right] \quad [9]$$

By using Eqs. [6] and [9], and defining a *tool geometry factor*,

$$\varphi = \frac{R_s^3 - R_p^3}{R_p^3 + 3\beta R_p^2 h_p} \quad [10]$$

The pin heat generation fraction [29] can be written as

$$f_{\text{pin}} = (\phi \varphi + 1)^{-1} \quad [11]$$

Equation [11] shows that the pin heat generation fraction relates to the tool friction factor  $\phi$  and tool geometry factor  $\varphi$ . Part I<sup>[29]</sup> reported that the friction coefficient approximately reads

$$\mu(T) = \mu_0 - K(T - 273) \quad [12]$$

$$\frac{\mu_0}{K} = T_{\text{melt}} - 273 \quad [13]$$

With the help of Eqs. [12] and [13], Eq. [8] yields

$$\phi = \frac{\mu(\bar{T}_s)}{\mu(\bar{T}_p)} = 1 - \frac{\bar{T}_s - \bar{T}_p}{T_{\text{melt}} - \bar{T}_p} \quad [14]$$

We assume that (a)  $\bar{T}_s$  equals the SC temperature  $T_{\text{center}}^s$  and (b)  $\bar{T}_p$  equals the PC temperature  $T_{\text{center}}^p$ . This is an approximation method. Then, with  $T_{\text{melt}} = 873$  K (600 °C) for 6061Al,<sup>[32]</sup> Eq. [14] yields

$$\phi = 1 - \frac{T_{\text{center}}^s - T_{\text{center}}^p}{873 - T_{\text{center}}^p} \quad [15]$$

and Eq. [9] reads

$$Q_{\text{total}} = \frac{\pi^2 \omega p}{45} \mu(T_{\text{center}}^p) \left[ \phi \left( R_s^3 - R_p^3 \right) + \left( R_p^3 + 3\beta R_p^2 h_p \right) \right] \quad [16]$$

The values of  $T_{\text{center}}^s$  and  $T_{\text{center}}^p$  can be found in Figure 5. Then the total heat generation and pin heat generation fraction can be calculated approximately by using Eqs. [16] and [11]. The computed results from this analytical method as well as the numerical results from the transient model are shown in Table II and Figure 6. Both analytically and numerically computed total heat generation and pin heat generation fraction show the

same variation trend. However, obvious differences can be observed. This is attributed to two reasons. First, it is difficult to specify the accurate values for  $\bar{T}_s$  and  $\bar{T}_p$ , which directly generate errors to the analytically computed results according to Eqs. [9] and [14]. Second, the friction heat contribution from the advancing movement is neglected, as can be seen from Eqs. [3] and [4] when the analytical method is used, whereas in the present numerical model, it is considered. Nevertheless, this approximation method gives us another understanding of the total heat generation  $Q_{\text{total}}$ , the pin heat generation fraction  $f_{\text{pin}}$ , and their correlations.

In detail, by combining the data shown in Table II and Figure 5, it can be seen that as the rotation rate increases from 900 to 1400 rpm,  $T_{\text{center}}^s$  ( $\approx \bar{T}_s$  according to the former assumption) increases from 691 K to 735 K (418 °C to 462 °C),  $T_{\text{center}}^p$  ( $\approx \bar{T}_p$  according to the former assumption) increases from 677 K to 719 K (404 °C to 446 °C),  $\mu$  decreases from 0.12 to 0.09,  $\phi$  decreases a little from 0.93 to 0.90, and, in turn, the total heat generation and pin heat generation fraction increase according to Eqs. [16] and [11]. These results can be summarized by the following two chains based on the *chain rule I with negative feedback mechanism*:<sup>[29]</sup>

$$\omega \uparrow: \left\{ \begin{array}{l} \frac{\bar{T}_s}{\bar{T}_p} \uparrow \xrightarrow[v, D_s, \text{and } D_p = \text{const}]{T - Cs} \left\{ \begin{array}{l} \phi \downarrow \\ \mu \downarrow \end{array} \right. \rightarrow Q_{\text{total}} \uparrow \end{array} \right. \quad [17a]$$

$$\omega \uparrow: \left\{ \begin{array}{l} \frac{\bar{T}_s}{\bar{T}_p} \uparrow \xrightarrow[v, D_s, \text{and } D_p = \text{const}]{T - Cs} \phi \downarrow \text{ a little} \\ \xrightarrow[\varphi = \text{constant}]{f_{\text{pin}} \approx \text{constant}} f_{\text{pin}} \approx \text{constant} \end{array} \right. \quad [17b]$$

where  $T - Cs$  is short for temperature conditions, which is  $T_{\text{center}}^s - T_{\text{center}}^p \approx \text{constant}$ ,  $T_{\text{center}}^p < 873$  K (600 °C), and  $(T_{\text{center}}^s - T_{\text{center}}^p) \ll (873 - T_{\text{center}}^p)$  and is also used in the following expressions. Evidence supporting Eqs. [17a] and [17b] can be found in Peel *et al.*'s work.<sup>[28]</sup> They reported that the heat generation increased from ~2100 to ~2600 W, and the friction coefficient decreased from ~0.57 to ~0.25 with increasing the rotation rate from 280 to 840 rpm at a constant advancing speed of 100 mm/min for FSW 5083-6082 dissimilar aluminum alloys.

Similar to Eqs. [17a] and [17b], the following two chains can be obtained:

$$v \uparrow: \left\{ \begin{array}{l} \frac{\bar{T}_s}{\bar{T}_p} \downarrow \xrightarrow[\omega, D_s, \text{and } D_p = \text{const}]{T - Cs} \left\{ \begin{array}{l} \phi \uparrow \text{ a litt} \\ \mu \approx \text{constant} \end{array} \right. \rightarrow Q_{\text{total}} \uparrow \end{array} \right. \quad [18a]$$

**Table II. Comparison of Analytically and Numerically Computed Results: Effects of Rotation Rate**

$\omega$ (rpm)	$\mu$	$\phi$	Total Heat Generation (W)		Relative Error (Pct)	Pin Heat Fraction		Relative Error (Pct)
			Analytical	Numerical		Analytical	Numerical	
900	0.12	0.93	2069	1900	8.9	0.227	0.138	64.5
1200	0.10	0.91	2322	2055	13.0	0.231	0.139	66.2
1400	0.09	0.90	2465	2130	15.7	0.233	0.140	66.4

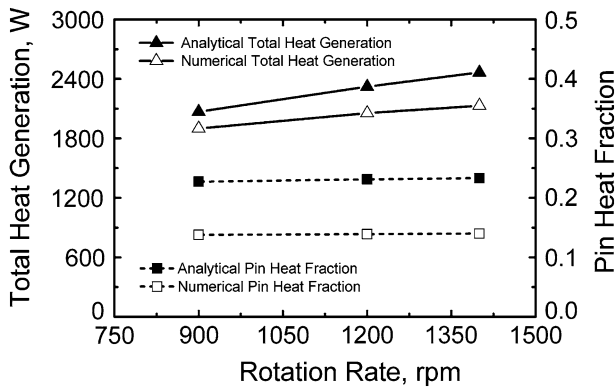


Fig. 6—Comparison between the analytical and numerical computed total heat generation, pin heat fraction: effects of rotation rate.

$$v \uparrow: \left\{ \begin{array}{l} \frac{\overline{T}_s}{\overline{T}_p} \downarrow \xrightarrow[\omega, D_s, \text{and } D_p = \text{const}]{T - C_s} \phi \uparrow \text{ a little} \\ \xrightarrow{\phi = \text{constant}} f_{\text{pin}} \approx \text{constant} \end{array} \right. [18b]$$

Peel *et al.*<sup>[28]</sup> also reported that the heat generation increased from ~2600 to ~3300 W and the friction coefficient retained an approximately constant value of ~0.25 with increasing the advancing speed from 100 to 300 mm/min at a constant rotation rate of 840 rpm for FSW 5083-6082 dissimilar aluminum alloys. This supports well the predictions by Eqs. [18a] and [18b]. Evidence from Reynolds *et al.*'s study<sup>[21]</sup> also supported the conclusion that the heat generation is proportional to the advancing speed. Furthermore, Yan *et al.*'s experimental research<sup>[33]</sup> and Arora *et al.*'s simulation study<sup>[20]</sup> provided further support to the positive linear correlation between heat generation and advancing speed. However, no literature has reported the heat generation data for various tool diameters. Here, the effect of the shoulder diameter and pin diameter on the heat generation is discussed.

$$D_s \uparrow: \left\{ \begin{array}{l} \frac{\overline{T}_s}{\overline{T}_p} \downarrow \xrightarrow[\omega, v, \text{and } D_p = \text{const}]{T - C_s} \left\{ \begin{array}{l} \phi \uparrow \text{ a little} \\ \mu \approx \text{constant} \end{array} \right\} \rightarrow Q_{\text{total}} \uparrow \\ D_s \uparrow \rightarrow R_s \uparrow \rightarrow R_s^3 \uparrow \end{array} \right. [19a]$$

$$D_s \uparrow: \left\{ \begin{array}{l} \frac{\overline{T}_s}{\overline{T}_p} \downarrow \xrightarrow[\omega, v, \text{and } D_p = \text{const}]{T - C_s} \phi \uparrow \text{ a little} \\ D_s \uparrow \rightarrow R_s \uparrow \rightarrow \phi \uparrow \end{array} \right\} \rightarrow f_{\text{pin}} \downarrow [19b]$$

$$D_p \uparrow: \left\{ \begin{array}{l} \frac{\overline{T}_s}{\overline{T}_p} \uparrow \xrightarrow[\omega, v, \text{and } D_s = \text{const}]{T - C_s} \left\{ \begin{array}{l} \phi \downarrow \text{ a little} \\ \mu \approx \text{constant} \end{array} \right\} \xrightarrow{\phi < 1} Q_{\text{total}} \uparrow \\ D_p \uparrow \rightarrow R_p \uparrow \rightarrow R_p^3 \uparrow \end{array} \right. [20a]$$

$$D_p \uparrow: \left\{ \begin{array}{l} \frac{\overline{T}_s}{\overline{T}_p} \uparrow \xrightarrow[\omega, v, \text{and } D_s = \text{const}]{T - C_s} \phi \downarrow \text{ a little} \\ D_p \uparrow \rightarrow R_p \uparrow \rightarrow \phi \downarrow \end{array} \right\} \rightarrow f_{\text{pin}} \uparrow [20b]$$

Equations [17] through [20] are the detailed expressions of *chain rule I with negative feedback mechanism*,<sup>[29]</sup> as it is used to explore the influence of welding parameters on the heat generation. Furthermore, these derivations reveal that (a) it is hard to specify a fixed value for the friction coefficient of the FSW process, because it is not a constant; and (b) with the effect of the *negative feedback mechanism*,<sup>[29]</sup> the FSW process can reach a thermal equilibrium whose level is affected by the variation of the welding conditions.

By using Eqs. [1] and [2], the heat generation data can be transformed into the torque and welding heat input. If the results of torque and the welding heat input can be validated, the heat generation can be verified indirectly. Furthermore, the present thermal model can be also verified indirectly. Evidence of the torque decreasing with increasing the rotation rate was also found in previous studies.<sup>[20,33,34]</sup> Arora *et al.*'s calculated results<sup>[20]</sup> indicated that with increasing the advancing speed, the torque increases linearly, whereas the welding heat input decreases rapidly. In addition, Yan *et al.*'s experimental results<sup>[33]</sup> showed a rapid decline in the torque with increasing the rotation rate from 150 to 480 rpm and a slow decline from 480 to 800 rpm for FSW 2524Al. They used the following sequence to explain this phenomenon: in the range from 150 to 480 rpm, the rotation rate was slow → the temperature of deformation material was low → the flow stress was high → the torque was high. In the range out of 480 rpm, the rotation rate was high → the temperature was high and almost reached a plateau value → further increase in the rotation rate only decreased the torque slightly. A further observation was found in Long *et al.*'s study.<sup>[34]</sup> They explained that the drop of flow stress with the temperature increase should be responsible for the torque drop. These studies provided a good foundation for supporting the present thermal model.

## B. Experimental Support from the HSZ-ITDL Model

The HSZ-ITDL model<sup>[12]</sup> revealed that the LHZ experienced a thermal history with a peak temperature of 643 K (370 °C) for the FSW 6061Al-T651. Thus, the location of the 643 K (370 °C) peak temperature contour computed in the present thermal model can be used to determine the location of the LHZ.

### 1. Characteristics of thermal cycles in LHZ

Thermal cycles of points A through C (defined in Figure 3(e)) for sample 24-8-900-200 along the 643 K (370 °C) peak temperature contour are shown in Figure 7. Obviously, three points are exposed to almost the same thermal cycles, which agree well with the HSZ-ITDL model.<sup>[12]</sup> To further explore the reason for this phenomenon, we can consider the temperature contour

fields in the horizontal plane ( $x$ - $y$  plane). If the thermal cycles of the three points are close to each other, the temperature contour fields of the three horizontal planes that contain points A through C should be almost the same. Furthermore, References 19 and 35 indicated that the thermal cycles can be constructed from the steady-state temperature field by transforming the distance traveled by the tool to time using the advancing speed. To show this, we can check a characteristic value of the thermal cycle, *i.e.*, the dissolution time  $t_d$ , which is

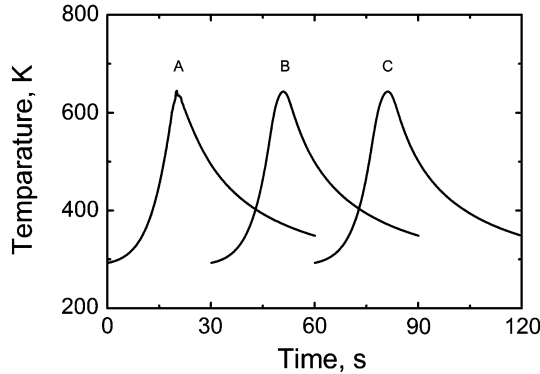


Fig. 7—Thermal cycles of points A, B, and C (defined in Fig. 3(e)) for sample 24-8-900-200.

important in controlling the precipitations. We can define a so-called dissolution displacement of the LHZ, which lies in the horizontal plane, parallel to the welding direction, tangent to the 643 K (370 °C) thermal contour, and enclosed by the 523 K (250 °C) thermal contour, *e.g.*, all the  $\overline{se}$ 's shown in Figure 8. If the advancing speed is  $v$ , the dissolution time  $t_d$  can be computed by

$$t_d = \frac{\overline{se}_i}{v} \quad [21]$$

where  $\overline{se}_i$  can be  $\overline{se}$ ,  $\overline{s'e'}$ , or  $\overline{s''e''}$ .

For sample 24-8-900-200, comparison between the computed dissolution times using Eq. [21] and the directly measured results from the thermal cycles of

**Table III. Comparison of Numerically and Analytically Computed Dissolution Times for Sample 24-8-900-200**

Points	$t_d$ (s)	
	From Computed Thermal Cycles	From Eq. [21]
A	10.6	10.6
B	11.6	11.6
C	12.0	12.0

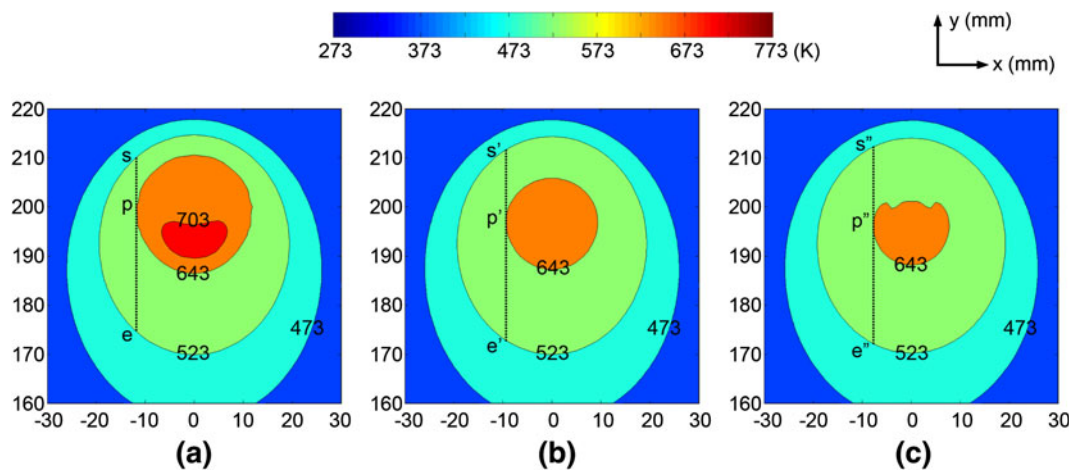


Fig. 8—Steady thermal contours of the (a) top plane, (b) middle plane, and (c) bottom plane of sample 24-8-900-200.

**Table IV. Comparison of the Computed and Measured 643 K (370 °C) Peak Temperature Contours**

Samples	Characteristic Length, $L$ (mm)		$\alpha$ (Deg)	
	Calculated	Experimental <sup>[12]</sup>	Calculated	Experimental <sup>[12]</sup>
24-8-1400-600	9.0	$9.0 \pm 0.5$	58	45 to 60
24-8-1400-400	10.3	$11.0 \pm 0.5$	62	52 to 68
24-8-1400-200	11.8	$13.0 \pm 0.5$	71	60 to 79
24-8-1200-200	11.2	$12.0 \pm 0.5$	61	58 to 78
24-8-900-200	9.2	$9.0 \pm 0.5$	52	58 to 78
20-10-1400-400	8.6	—	61	—
20-8-1400-400	8.4	$9.0 \pm 0.5$	60	51 to 67
20-6-1400-400	8.2	$9.0 \pm 0.5$	59	45 to 60
16-8-1400-400	6.2	$7.0 \pm 0.5$	58	60 to 78

the three points are shown in Table III. The results obtained from two different methods are the same. To summarize, the reason for different locations along the 643 K (370 °C) peak temperature contour in a weld having similar thermal cycles is that they experience almost the same thermal excursion. One point to be

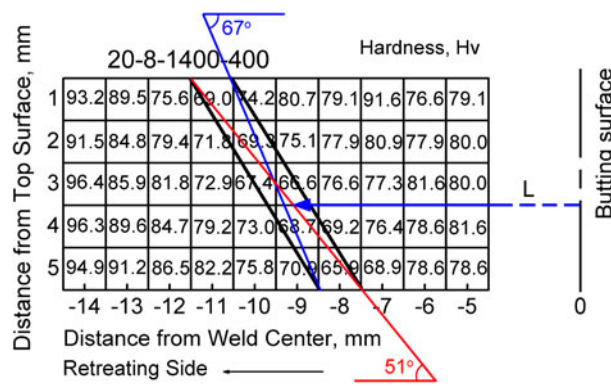


Fig. 9—Illustration of LHZ.<sup>[12]</sup> Two black oblique lines are boundaries of LHZ, and the red and blue lines are lower and upper limits of LHZ inclination.  $L$  is the characteristic length describing the location of LHZ.

noted is that this formula is limited to the steady welding period.

## 2. Influence of weld conditions on 643 K (370 °C) peak temperature contour

Table IV shows the comparison of the geometry characteristics between the 643 K (370 °C) peak temperature contour (defined in Figure 3(e)) and the experimentally measured LHZ characteristics,<sup>[12]</sup> which was determined by constructing the hardness distribution map around the HAZ throughout the entire thickness of the welded workpiece, as shown in Figure 9. Good agreement can be observed in both location and inclination.

It can be observed that increasing the rotation rate, shoulder diameter, and pin diameter and decreasing the advancing speed move the LHZ outward from the butting surface. This is because these variations of the welding conditions increase the welding heat input (Figure 2), and then, in turn, the maximum temperature (Figure 5) as well as the whole temperature level. Furthermore, as the advancing speed decreases from 600 to 200 mm/min, the welding heat input increases by 353 J/mm (Figure 2(b)) and the distance of the 643 K (370 °C) peak temperature contour from the butting

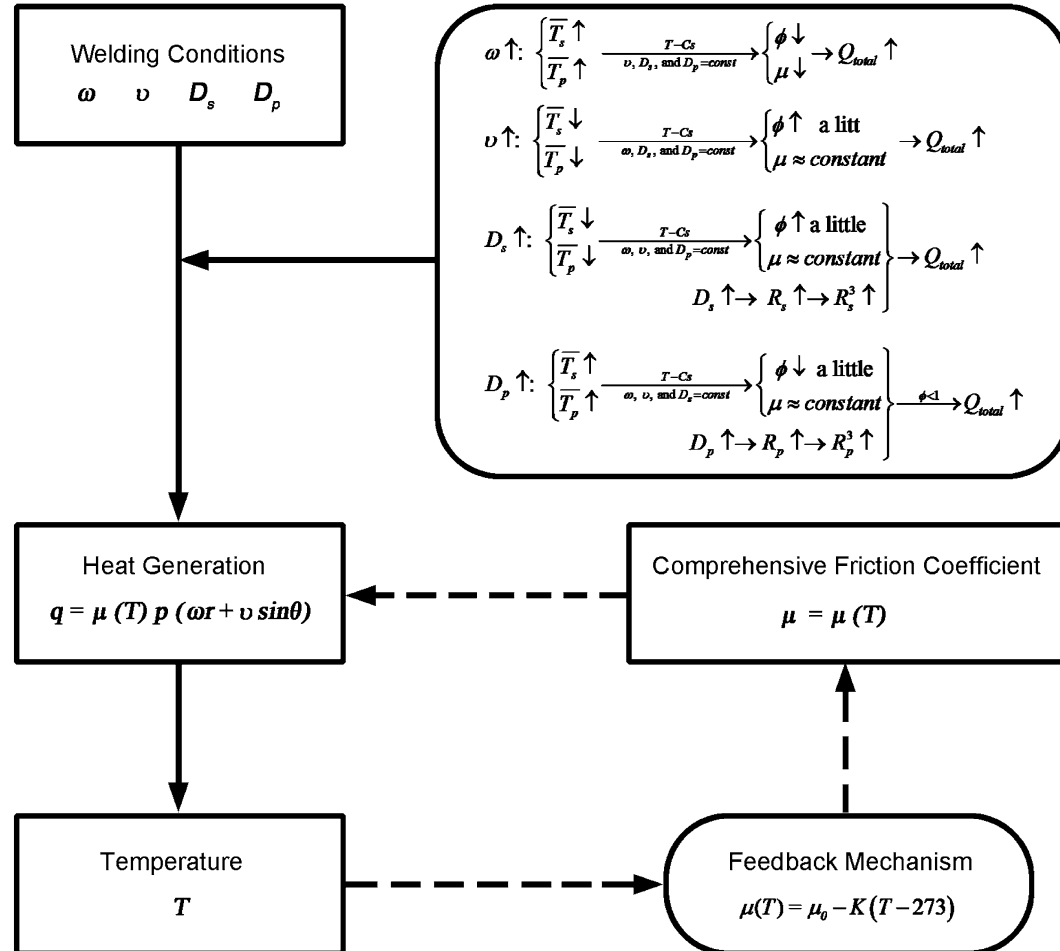


Fig. 10—Relationship between the welding parameters and temperature for FSW 6061Al. Dash arrows mean that they are taken from Part I<sup>[29]</sup> to complete the relationship map.

surface increases by 2.8 mm (Table IV). However, as the shoulder diameter increases from 16 to 24 mm, the weld heat input increases by only 70 J/mm (Figure 2(c)), but the distance of the 643 K (370 °C) peak temperature contour from the butting surface increases by 4.1 mm (Table IV). It can be seen that the move of the peak temperature contour is dependent on not only the welding heat input but also the shoulder diameter. Increasing the shoulder diameter increases the area of heat source and, in turn, the distribution area of the welding heat input. In conclusion, the distance of the 643 K (370 °C) peak temperature contour (or LHZ) from the butting surface is affected by both the welding heat input and the shoulder diameter.

## V. CONCLUSIONS

Within the range of the welding conditions studied in the present article, the following conclusions can be summarized.

1. The heat generation increases with increasing all the parameters, *i.e.*, rotation rate, advancing speed, shoulder diameter, and pin diameter. The welding heat input increases with increasing the rotation rate, shoulder diameter, and pin diameter, but decreases quickly with increasing the advancing speed. The torque increases with increasing the advancing speed, shoulder diameter, and pin diameter, but decreases with increasing the rotation rate.
2. The dissolution time increases slowly with increasing the rotation rate, shoulder diameter, and pin diameter, but decreases quickly with increasing the advancing speed.
3. The temperature contour moves away from the butting surface, which is the prime reason why the LHZ and fracture path<sup>[12]</sup> move away from the butting surface, with increasing the rotation rate and shoulder diameter, decreasing the advancing speed. The pin diameter only has a slight impact on the temperature contour. The location of the temperature contour is affected by both the welding heat input and the shoulder diameter.
4. The relationship between weld conditions, heat generation, temperature, and friction coefficient can be summarized in the relationship map as shown in Fig. 10.

## ACKNOWLEDGMENTS

The authors gratefully acknowledge the support of (a) the National Outstanding Young Scientist Foundation of China under Grant No. 50525103 and (b) the Hundred Talents Program of the Chinese Academy of Sciences.

## NOMENCLATURE

$D_p, D_s$	pin, shoulder diameter (mm)
$E$	weld heat input (J/mm)

$h_p$	pin length (mm)
$K$	curve fitting slope
$L$	characteristic length (mm)
$M$	torque (Nm)
$P$	pressure (Pa)
$q$	heat generation rate ( $\text{J mm}^{-3}$ )
$Q_p, Q_s, Q_{total}$	pin, shoulder and total heat generation (W)
$R_p, R_s$	pin, shoulder radius (mm)
$r$	radius (mm)
$T$	temperature (K)
$T_{melt}$	melting point (K)
$T_p^*$	temperature in pin/matrix interface (K)
$T_p$	temperature (K), $T_{p,\max} < T_p < T_{p,\min}$
$T_s$	temperature in shoulder/matrix interface (K)
$\bar{T}_s$	temperature (K), $T_{s,\max} < \bar{T}_s < T_{s,\min}$
$T_{center}^s$	temperature at the SC (K)
$T_{center}^p$	temperature at the PC (K)
$t_d$	dissolution time (s)
$v$	advancing speed ( $\text{mm min}^{-1}$ )
$x, y, z$	coordinate axes
$\beta$	pin contact coefficient for treaded pin
$\mu_0$	curve fitting intercept
$\mu$	comprehensive friction coefficient
$\theta$	angle (rad)
$\omega$	rotation rate (rpm)
$\pi$	$\text{Pi}$

## REFERENCES

1. R.S. Mishra and Z.Y. Ma: *Mater. Sci. Eng. R*, 2005, vol. 50, pp. 1–78.
2. C.G. Rhodes, M.W. Mahoney, W.H. Bingel, R.A. Spurling, and C.C. Bampton: *Scripta Mater.*, 1997, vol. 36, pp. 69–75.
3. M.W. Mahoney, C.G. Rhodes, J.G. Flintoff, R.A. Spurling, and W.H. Bingle: *Metall. Mater. Trans. A*, 1998, vol. 29A, pp. 1955–64.
4. Y.S. Sato, H. Kokawa, M. Enmoto, and S. Jogan: *Metall. Mater. Trans. A*, 1999, vol. 30A, pp. 2429–38.
5. Y.S. Sato, M. Urata, and H. Kokawa: *Metall. Mater. Trans. A*, 2002, vol. 33A, pp. 625–35.
6. P. Cavaliere, G. Campanile, F. Panella, and A. Squillace: *J. Mater. Process. Technol.*, 2006, vol. 5, pp. 263–70.
7. W.B. Lee, Y.M. Yeon, and S.B. Jung: *Mater. Trans.*, 2004, vol. 45, pp. 1700–05.
8. S.G. Lim, S.S. Kim, C.G. Lee, and S.J. Kim: *Metall. Mater. Trans. A*, 2004, vol. 35A, pp. 2829–35.
9. S.R. Ren, Z.Y. Ma, and L.Q. Chen: *Scripta Mater.*, 2007, vol. 56, pp. 69–72.
10. A. Scialpi, L.A.C. De Filippis, and P. Cavaliere: *Mater. Des.*, 2007, vol. 28, pp. 1124–29.
11. H. Fujii, L. Cui, M. Maeda, and K. Nogi: *Mater. Sci. Eng. A*, 2006, vol. A419, pp. 25–31.
12. F.C. Liu and Z.Y. Ma: *Metall. Mater. Trans. A*, 2008, vol. 39A, pp. 2378–88.
13. H.B. Schmidt and J.H. Hattel: *Scripta Mater.*, 2008, vol. 58, pp. 332–37.
14. J.H. Kim, F. Barlat, C. Kim, and K. Chung: *Metall. Mater. Int.*, 2009, vol. 15, pp. 125–32.
15. S. Xu, X. Deng, and A.P. Reynolds: *Sci. Technol. Weld. Join.*, 2001, vol. 6, pp. 191–93.
16. H. Schmidt and J. Hattel: *Model. Simul. Mater. Sci. Eng.*, 2005, vol. 13, pp. 77–93.
17. Q.Z. Zhang, L.W. Zhang, W.W. Liu, X.G. Zhang, W.H. Zhu, and S. Qu: *Sci. Technol. Weld. Join.*, 2006, vol. 11, pp. 737–43.

18. Z. Zhang and H.W. Zhang: *Int. J. Adv. Manuf. Technol.*, 2008, vol. 37, pp. 279–93.
19. R. Nandan, G.G. Roy, T.J. Lienert, and T. DebRoy: *Acta Mater.*, 2007, vol. 55, pp. 883–95.
20. A. Arora, R. Nandan, A.P. Reynolds, and T. DebRoy: *Scripta Mater.*, 2009, vol. 60, pp. 13–16.
21. A.P. Reynolds, W. Tang, Z. Khandkar, J.A. Khan, and K. Lindner: *Sci. Technol. Weld. Join.*, 2005, vol. 10, pp. 190–99.
22. Y.J. Chao and X. Qi: *Proc. 1st Int. Symp. on Friction Stir Welding*, TWI, Thousand Oaks, CA, June 1999, pp. 31–38.
23. Ø. Frigaard, Ø. Grong, and O.T. Midling: *Metall. Mater. Trans. A*, 2001, vol. 32A, pp. 1189–98.
24. M. Song and R. Kovacevic: *Int. J. Mach. Tools. Manuf.*, 2003, vol. 43, pp. 605–15.
25. M.Z.H. Khandkar, J.A. Khan, and A.P. Reynolds: *Sci. Technol. Weld. Join.*, 2003, vol. 8, pp. 165–74.
26. H. Schmidt, J. Hattel, and J. Wert: *Model. Simul. Mater. Sci. Eng.*, 2004, vol. 12, pp. 143–57.
27. H. Schmidt and J. Hattel: *Sci. Technol. Weld. Join.*, 2005, vol. 10, pp. 176–86.
28. M.J. Peel, A. Steuwer, P.J. Withers, T. Dickerson, Q. Shi, and H. Shercliff: *Metall. Mater. Trans. A*, 2006, vol. 37A, pp. 2183–93.
29. X.X. Zhang, B.L. Xiao, and Z.Y. Ma: *Metall. Mater. Trans. A*. DOI: [10.1007/s11661-011-0729-5](https://doi.org/10.1007/s11661-011-0729-5).
30. P. Colegrove, M. Pinter, D. Graham, and T. Miller: *Proc. 2nd Int. Symp. on Friction Stir Welding*, TWI, Gothenburg, Sweden, June 2000, pp. 26–28.
31. Q. Shi, T. Dickerson, and H.R. Shercliff: *Proc. 4th Int. Symp. on Friction Stir Welding*, TWI, Park City, UT, May 2003, pp. 14–16.
32. *Recommended Values of Thermophysical Properties for Selected Commercial Alloys*, C.M. Kenneth, ed., Woodhead Publishing Ltd., Cambridge, England, 2002.
33. J.H. Yan, M.A. Sutton, and A.P. Reynolds: *Sci. Technol. Weld. Join.*, 2005, vol. 10, pp. 725–36.
34. T. Long, W. Tang, and A.P. Reynolds: *Sci. Technol. Weld. Join.*, 2007, vol. 12, pp. 311–17.
35. K. Mundra, T. DebRoy, and K.M. Kelkar: *Numer. Heat Transfer A*, 1996, vol. 29, pp. 115–29.